Mechanical and Electrical Alignment Techniques for Plane-Polar Near-Field Test Systems

Michael Carey, Patrick Pelland, Stuart Gregson
Nearfield Systems Inc.
Torrance, CA, USA

Naoki Shinohara
Research Institute for Sustainable Humanosphere
Kyoto University
Kyoto, Japan

***Abstract*— The planar near-field technique is one of the most widely used, methods for measuring electrically large, medium to high gain antennas [1, 2]. Plane rectilinear systems consist of two intersecting, orthogonal linear translation stages which produces data in a convenient regularly spaced rectilinear co-ordinate system. Although the plane rectilinear geometry is by far the most commonly encountered implementation, plane-polar [2, 3] and plane-bipolar [4] geometries can also be constructed using mechanically convenient, commercially available, positioners. Plane-polar acquisition systems typically comprise the intersection of a rotation stage mounted behind the AUT, with a linear probe translation stage acting as a radial arm. This geometry yields data tabulated in a plane-polar co-ordinate system. Although comparatively rare in industry, plane-polar systems are important because they present certain distinct advantages [3, 5]. They do however pose some unique challenges within their implementation. As with all near-field methodologies, accurate and precise probe positioning is of paramount importance to the success of the technique and comprises an important term within the facility level uncertainty budget [6, 7]. Clearly, this is equally valid for the planar-polar technique with the hybrid angular/linear positioning system presenting unique challenges to the mechanical alignment.**

This paper will describe newly developed mechanical and electrical alignment techniques for use with plane-polar near-field test systems. A simulation of common plane-polar alignment errors will illustrate, and quantify, the alignment accuracy tolerances required to yield high quality far-field data, as well as bounding the impact of highly repeatable systematic alignment errors. The new plane-polar electrical alignment technique comprises an adaptation of the existing, widely used, spherical near-field electrical alignment procedure [8] and can be used on small, and large, plane-polar near-field antenna test systems.

I. Introduction

Plane-polar acquisition systems typically consist of a rotation stage mounted behind the AUT whose axis of rotation is orthogonal to a linear probe translation stage acting as a radial arm. This geometry yields data tabulated in a plane-polar co-ordinate system. In addition, a polarisation rotator mounted behind the probe is typically present to permit dual-polarised measurements. While plane-polar theory and measured results have been presented and validated [3, 4, 5], a detailed alignment procedure has never surfaced in the literature. This paper will present a generalized alignment procedure for horizontal plane-polar near-field systems. In Sections II and III, a set of alignment requirements will be shared along with a collection of required tools. Section IV will present a detailed mechanical alignment procedure for two variations of horizontal plane-polar systems. The first configuration places the AUT rotator at the edge of radial travel as shown in Figure 1. The second configuration places the AUT rotator at the center of radial travel as shown in the NSI delivered plane polar scanner at Kyoto University (Figure 2). Once the mechanical alignment procedure has been presented, Section V will illustrate the effects of alignment errors in plane-polar measurements on far-field data using a near-field simulation tool. Finally, some conclusions will be presented in Section VI.

Figure 1. NSI-920PP-6 Horizontal Plane Polar System with 1.8 m Radial Translation Axis

II. Scanner Alignment Requirements

In order to perform valid plane-polar near-field measurements several fundamental alignment requirements must be met:

1. The near-field probe should travel along a linear translation stage (radial axis) while maintaining a constant position in both transverse directions.
2. The vector of the scanner's phi axis rotator should be orthogonal to the direction of probe travel.
3. The vector of the probe's polarisation rotator should also be orthogonal to the radial axis.
4. The position of the probe along the radial axis where the scanner's polarisation and phi axes are coincident should be defined as its zero position, r_0.

Figure 3 shows a diagram of a horizontal plane-polar near-field system. In this image, the radial axis is positioned orthogonal to gravity and lies along the *y* axis. The probe's polarisation axis points in the direction *–z* while the phi axis points to *+z*, parallel to gravity and orthogonal to the radial axis. In this configuration, the probe travels over a finite linear span, $- r_{max} \leq r \leq r_{max}$ at $x = 0$. Figure 1 shows a different configuration of plane-polar near-field scanner where $0 \leq r \leq r_{max}$. Both are valid plane-polar near-field configurations, provided the Nyquist sampling rate is not violated.

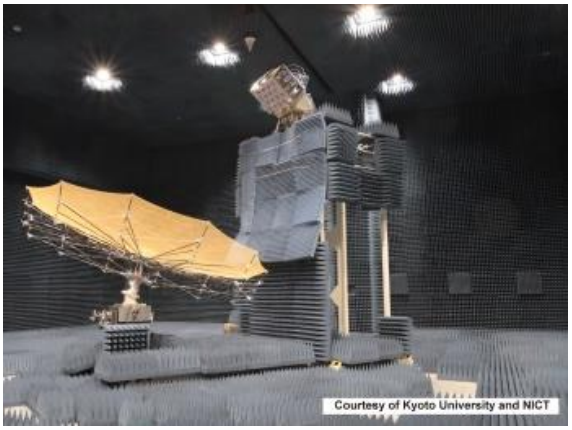

Figure 2. Kyoto University Plane Polar System with a 6 m Radius (12 m Diameter) Translation Axis

Installation of the near-field scanner in the horizontal orientation as shown in Figures 1 through 3 greatly simplifies the alignment procedure, allowing one to use gravity as a reference vector. This paper will detail the alignment procedure for these types of plane-polar systems, specifically.

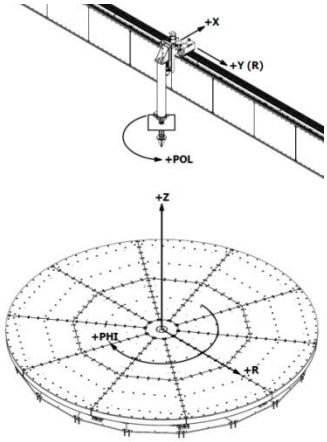

Figure 3. Plane-Polar Schematic showing Coordinate System and Three Axes of Motion

III. Alignment Tools Required

Traditional methods of aligning near-field systems involve the use of optical tooling including jig transits, theodolites, optical cubes, mirrors, etc. More recently, laser trackers have been used to perform alignment tasks. Alignment using these tools is difficult, time consuming, and requires the services of persons experienced with the tools' use to obtain useful results [8].

The procedure described here makes use of the high accuracy, low cost five axis laser alignment unit shown in Figure 4. It produces five orthogonal beams from a single laser source. These tools typically offer accuracies on the order of +/- 6 mm @ 30 m distance, translating to roughly 0.011°. One of the most important features of this tool is that it is able to self-level its internal laser source, producing two beams parallel to gravity and three beams orthogonal to gravity. A simple recalibration procedure is provided by the manufacturer to ensure that these conditions are met. Performance of this unit has been confirmed by measuring the beam deviation using a laser tracker [8].

Figure 4. Five Axis Laser Alignment Tool

The tools and equipment required to align horizontal plane-polar scanners are summarized in Table I.

TABLE I. Plane-Polar Alignment Tools Required

Tool	Use
Five Axis Laser Unit	Provides self-levelling laser reference aligned to gravity
Telescoping Stand	Mounts the five axis laser
Precision Machinist Level	Levels radial axis and rotation stages
Axis Location Plate Tool	Locates the axis of rotation of the phi and polarisation axes
Front Surface Mirror	Measures the pointing angle of the two rotation stages
Assorted Shim Stock	Makes fine mechanical adjustments to pointing of rotation stages

IV. Mechanical Alignment Procedure

A. Horizontal Leveling of the Radial Axis

For the horizontal plane-polar near-field configurations discussed in this paper, the first goal is to ensure that the radial axis is aligned orthogonal to gravity.

For small, self-contained scanners like the one shown in Figure 1, this can be accomplished by first rough levelling the entire plane-polar structure in both *x* and *y* directions by adjusting the feet at the base of the structure. Ensure that the load is distributed evenly across the feet to eliminate any potential rocking and then make fine adjustments to level the radial arm along the *y* axis to within 0.005°. For larger scanners like the one shown in Figure 2, the radial axis may be mounted to large support columns or integrated into the

building construction. For these systems, great care must be taken during installation as re-adjusting the level of the guide rail may prove difficult in the future. When convenient, the use of appropriately sized shims may be used to fine tune the level of the radial axis.

Figure 5 shows a technique to check the level of the radial axis for a downward facing guide rail using a machined flat plate and precision mechanic's level. The plate is held up against the guide rail and the level is placed on the flat plate. Inspect the flat plate for burrs or raised edges. It must be flat to obtain an accurate level. If the guide rail is upward facing, the level may be placed directly on the surface. The levelling and checking procedure is repeated until the rail is aligned to within 0.005°. Once complete, the guide rail on the underside of the structure is levelled and the *y* axis of the scanner's coordinate system has been defined.

Figure 5. Checking the Radial Axis Level

B. Locating r_0 Position Along the Radial Axis

To make the most efficient use of the radial axis' total available travel, the location of the probe's $r = 0$ position should be optimized. For the case where $0 \leqslant r \leqslant r_{max}$, the $r = 0$ position should be defined at the furthest possible point along the *y* axis in the negative direction. This will provide the largest possible value of r_{max}, thereby maximizing the measurement potential for a fixed length linear axis.

When the position of r_0 is to be located at the center of travel, $-r_{max} \leqslant r \leqslant r_{max}$, special techniques should be used to locate $r = 0$. Here, an automated process was used to determine total travel available and locate the exact center. This process ensures that the probe may travel equidistant in both the positive and negative directions to maximize the scanner's potential.

Once the r_0 position of the scanner has been determined the five axis laser unit should be placed in such a manner that its upward pointing beam illuminates the polarisation axis of rotation, as shown in Figure 6. Here, an axis alignment plate is mounted directly to the rotation stage to provide a precise reference point that defines the center of rotation. When the upward pointing laser beam is illuminating the center of the reference point, great care should be taken to ensure that the five axis laser unit is not disturbed. The self-levelling feature of the tool ensures that the downward pointing beam now illuminates the location where the phi axis rotator should be installed.

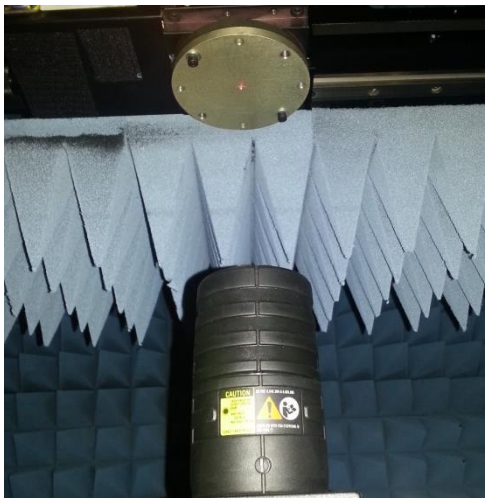

Figure 6. Axis Location Plate Mounted to Polarisation Rotator to Position Five Axis Laser Tool

C. Probe Polarisation Stage Pointing

With the probe's $r = 0$ having been defined in the previous step, the pointing of the polarisation axis must be adjusted to ensure that the stage's axis of rotation is vertical and orthogonal to the linear axis.

Attach a front surface mirror to the platen of the polarisation rotator similar to Figure 8, where the mirror is attached to the AUT's phi axis of rotation. In this case, the front surface mirror is mounted to the axis location plate discussed in the previous section. Observe the reflection of the laser beam back onto its source. Rotate the polarisation axis and note the shape and location of the reflected beam that is drawn by the laser beam back at the source. Shim the polarisation stage until the reflected beam is perfectly coincident with the outgoing beam.

Remove the mirror from the axis location plate and confirm that the upward pointing beam is still illuminating the target. If large adjustments to the pointing of the polarisation axis were required, the five axis laser position may need to be changed. Re-position the five axis alignment tool so that it is once again directly below the polarisation axis' center of rotation. Re-install the mirror and iterate as necessary.

D. Positioning the Phi Axis at Center of the Radial Axis

At this point, the radial axis has been levelled with respect to gravity and the r_0 position of the probe has been defined in order to maximize the total available travel. The five axis laser should be positioned so that its upward facing beam is pointing at the axis alignment target on the polarisation stage rotator. The vertical laser beam now defines the $(x,y) = (0,0)$ position of the scanner's coordinate system and should remain undisturbed for the remainder of the alignment process.

The phi stage should now be installed in a position close to $(x,y) = (0,0)$ but not yet secured in place. Once installed, the axis location plate can be removed from the probe's polarisation rotator and moved to the AUT's phi stage. Alternatively, a second plate may be used to reduce the amount of required setup re-configuration. The phi stage may now be translated along the *x* and *y* axes until the downward facing

laser beam points to the target on the axis location plate, as shown in Figure 7. At this point, the phi stage must be secured in place.

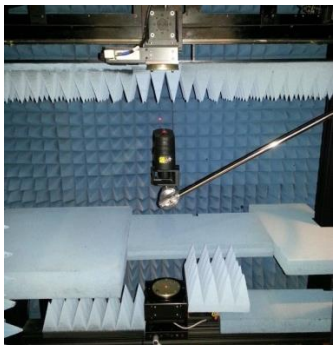

Figure 7. Five Axis Laser Used to Set Position of Phi Axis Below Probe's *r0* Position

E. Phi Stage Pointing

Now that the phi stage has been placed at (x,y) = (0,0), the same procedure outlined in sub-section C. should be followed to ensure that the AUT's phi axis vector is aligned to gravity.

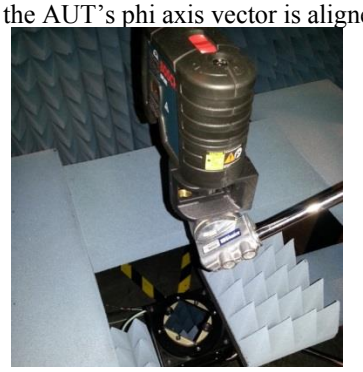

Figure 8. Front Surface Mirror Mounted to Phi Axis to Determine Pointing Error

V. PLANE POLAR NEAR-FIELD SIMULATION

The development of general-purpose tools for the computational electromagnetic (CEM) simulation of near-field or far-field antenna measurements is of interest for many reasons. Such a tool would enable one to: plan and optimise a measurement campaign before committing valuable facility time or resources, or to assess individual error terms within the facility level error budget, or to verify correction algorithms. In this study a near-field simulation was constructed using standard plane-wave spectrum methods to reconstruct near-fields from measured far-field data.

It is widely known that an angular spectrum of plane waves can be obtained directly from sampled tangential near-field components using [1, 2, 5],

$$F(k_x,k_y)=\int_0^{2\pi}\int_0^{\infty} f(r,\phi)e^{jk_0 r(u\cos(\phi)+v\sin(\phi))}r\,dr\,d\phi \qquad (1)$$

It is also known that, from an application of the stationary phase algorithm [2], the asymptotic far electric fields can be easily obtained from the angular spectrum of plane waves since as $r\to\infty$ [2],

$$\underline{E}(k_x,k_y)\approx j\frac{e^{-jk_0 r}}{\lambda r}\frac{k_z}{k_0}\left[\underline{F}_T(k_x,k_y)-\frac{\underline{k}_T\cdot\underline{F}_T(k_x,k_y)}{k_z}\hat{e}_z\right] \qquad (2)$$

The corresponding near-fields at any point in the forward half-space space (*x*, *y*, *z*) can be recovered from the plane wave spectrum (PWS) from an inversion of equation (1) [2],

$$\underline{E}(x,y,z)=\frac{1}{4\pi^2}\int_{-k_{y0}}^{k_{y0}}\int_{-k_{x0}}^{k_{x0}}\underline{F}(k_x,k_y,z=0)e^{-jk_0(ux+vy+wz)}dk_x dk_y \qquad (3)$$

Where, $k_{x0} = k_{0y} = 2\pi/\lambda$. Thus, providing reference far electric fields are available, perhaps from an auxiliary spherical measurement or from a full wave CEM solver, then it is possible to use an inversion of equation (2) to compute the plane-wave spectra from the far electric fields before using equation (3) to synthesise near-fields across a regular plane-polar co-ordinate system where $x = r\cos\phi$, $y = r\sin\phi$, with *z* arbitrary but fixed. This procedure was used to simulate data tabulated on a plaid monotonic and equally spaced (in each axis) plane-polar grid with the near-field being specified as though the probe had been counter rotated (*i.e.* in a Ludwig III type acquisition scheme [5]) so that the AUT and probe fields remain polarisation matched for the duration of the near-field scan. The AUT-to-probe separation was three wavelengths so as to be outside the reactive near-field region. This is an acquisition mode that is often used in practice and was adopted here for the sake of consistency. Near-field simulations were produced using two commonly utilised acquisition schemes with the intension of examining the behaviour that specific alignment errors have on the asymptotic far-field parameters as obtained using various acquisition modes. These modes were:

1) $0\le r\le r_{MAX}$, $-\pi\le\phi\le\pi$, (360° ϕ acquisition),

2) $-r_{MAX}\le r\le r_{MAX}$, $0\le\phi\le\pi$, (180° ϕ acquisition).

Taking a narrow beam, slotted waveguide array, with a gain of 35 dB as the AUT with an operating frequency of 9.375 GHz, plane-polar near electric fields were simulated for each of these modes with varying r_0 errors being introduced into the simulation. The equivalent far-fields were then determined using standard plane-polar near-field to far-field transformation techniques [2, 5]. This antenna was linearly polarized with an on-axis axial ratio of greater than 40 dB. Here, the r_0 error was defined to be the linear distance between the zero on the linear scan axis (i.e. the point that is defined to be the pole of the plane-polar co-ordinate system $r = 0$), and the true point where the rotation axis actually intersects with the linear-axis. This error term was selected as in practice this had been found to be difficult to determine accurately and appeared to have a significant impact on the uncertainty budget. Figure 9 below contains the great circle cardinal cut as obtained from the 360° ϕ acquisition data with r_0 errors ranging from 0 (ideal reference), λ/20, λ/10, λ/5, and λ/2 respectively. From inspection of these figures it is clear that the peak of the pattern has noticeably reduced as the r_0 error increased. This is also shown in Figure 10 in which the axes of the plot have been adjusted so as to focus on the main beam region of the antenna patterns. From inspection of this figure, it is evident that a comparatively small r_0 error, *i.e.* one twentieth of a wavelength resulted in a reduction in the peak pattern level of *circa* 0.1 dB. This would correspond to a comparatively large component in the overall gain uncertainty budget. Furthermore, as the r_0 error increased, the location of the sidelobes progressively shifted to wider angles. This behaviour was expected as larger

r_0 errors result in an apparent reduction in the spatial extent of the AUT thereby reducing the measured gain value and increasing the beam-width of the observed far-field pattern.

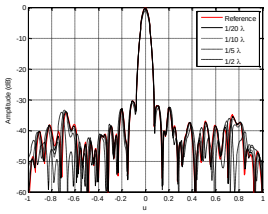

Figure 9. Far-Field Cardinal Cut of 360° ϕ Measurements Showing Pattern for Various r0 Errors.

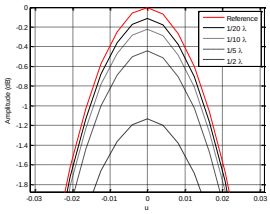

Figure 10. Far-Field Cardinal Cut of 360° ϕ Measurements Showing Beam Peak for Various r_0 Errors.

Figure 11 and Figure 12 contain equivalent far-field patterns to Figure 9 and Figure 10 above only here the far-field patterns were obtained from the 180° ϕ acquisition.

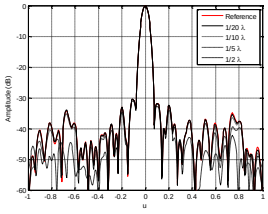

Figure 11. Far-Field Cardinal Cut of 180° ϕ Measurements Showing Pattern for Various r_0 Errors.

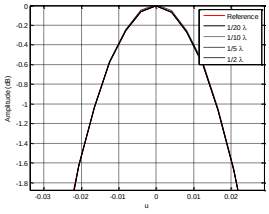

Figure 12. Far-Field Cardinal Cut of 180° ϕ Measurements Showing Beam Peak for Various r_0 Errors.

From inspection of Figure 12 it is evident that the peak level is *far* less sensitive to the r_0 error than was the case for 360° ϕ scan data. As before the location of the sidelobes varies with the r_0 error exhibiting similar behaviour to the 360° ϕ scan data. The apparent insensitivity in peak level to the r_0 error for the 180° ϕ scan data requires further examination as this behaviour it is perhaps not immediately apparent. One explanation for this behaviour can be obtained by comparing and contrasting respective the near-field pattern plots for these acquisition modes. Figure 13 contains the plane-polar near-field data presented in the form of a Cartesian co-ordinate system for the case where no r_0 error is present. Here, a -20 dB contour has been added to this false colour checkerboard plot to provide a visual aid in determining the spatial extent of the majority of the radiated fields. Figure 14 and 15 contain equivalent plots for the 180° and 360° ϕ scan cases where an r_0 = 1λ error has been introduced.

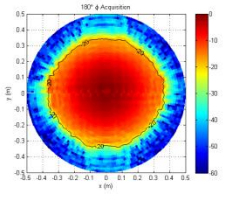

Figure 13. 180° ϕ Scan with no r_0 Error.

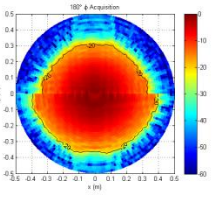

Figure 14. 180° ϕ Scan with r_0 Error.

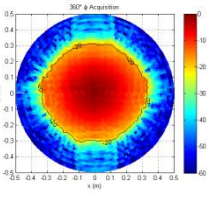

Figure 15. 360° ϕ Scan with r_0 Error.

When there is no r_0 error the 180° and 360° ϕ scans result in the same near-field patterns. However from inspection, we can see that as the r_0 error gets larger, for the case of the 360° ϕ scan the area of the AUT decreases. Conversely, for the case of the 180° ϕ scan, one half of the near-field measurement the area of the AUT decreases, however for the opposite half of the acquisition the area increases. Again, this is illustrated by the -20 dB contour. This makes sense from the scan type standpoint since for the case of a 180° ϕ scan mode, a r_0 error merely displaces the AUT in each individual cut with the true "width" of the illumination being preserved as the AUT is, in essence, merely translated linearly from its true position. This is not the case for the 360° scan in which the AUT is apparently shrunk (or conversely enlarged depending on the sign of the r_0 error) with radiated energy being omitted from the measurement. Clearly, although preserving the area of the near-field illumination within the 180° ϕ scan will yield a more stable far-field peak, a consequence of the non-physical discontinuity in that near-field illumination will inevitably result in the appearance of spurious high angular frequency sidelobes in the far-field.

VI. Using Measured Data to Refine r_0

As illustrated above, the mechanical ϕ-axis rotator must be correctly aligned with the linear axis and the probe placed in the proper location when performing plane-polar near-field measurements. In some cases it may be impractical to place the optical alignment equipment on the AUT or optical instruments may not be available. In these cases, it may be desirable to check the alignment using electrical measurements on the actual AUT and probe. Appropriate comparison and analysis of two near-field measurements (which can be extracted from a carefully orchestrated single acquisition) that should be identical yield precise measures of some rotator and probe alignment errors. While in principle these tests are independent of the AUT pattern, as will be illustrated below, judicious choice or placement of the antenna can significantly increase the sensitivity of this procedure. Careful examination of the 180° ϕ scan acquisition, and recalling the mapping from the "alternate" (or second) plane to the conventional (or first) plane can be expressed mathematically as, $r \rightarrow -r$ and $\phi \rightarrow \phi \pm \pi$ we can see that the ϕ = 180° cut represents a repeat measurement of the ϕ = 0° cut. This can be seen illustrated in Figure 16 below which contains a comparison of ϕ = 0° and ϕ = 180° cuts showing effect of r_0 error on near-field data. That is to say, the point on the linear scan axis that is defined to be zero is not coincident and synonymous with the ϕ rotation axis. The misalignment is clear from this "flip" test. Perhaps the simplest and most reliable method for determining the displacement between these patterns is to determine the spectral content and examine the relative phase difference. An alternative approach would be to interpolate the measured patterns to sequentially shift the respective patterns and to assess the correspondence by evaluating the cross-correlation coefficient however as will be shown below, the spectral method is a more direct, noise suppressing technique. The one dimensional spectral content of the cut can be obtained by evaluating the one-dimensional Fourier transform [2] using,

$$F(u) = \int_{-\infty}^{\infty} f(r) e^{jk_0 ur} dr \qquad (4)$$

Here, the range of the one-dimensional integral collapses so that the Dirichlet conditions [2] and the Nyquist [2] sampling

conditions are satisfied, which would be the case for any conventional near-field measurement from which conceivably this data would be extracted. The resulting magnitude and phase spectra can be seen presented in Figure 17 and 18 respectively where the red traces denote spectra arising from the $\phi = 0°$ cut and the black traces denote spectra from the $\phi = 180°$ cut.

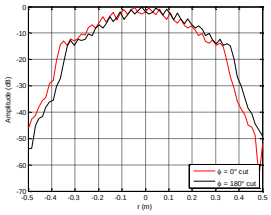

Figure 16. Comparison of $\phi = 0°$ and $\phi = 180°$ Cuts Showing Effect of r_0 Error on Near-Field Data.

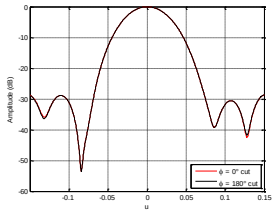

Figure 17. Comparison of $\phi = 0°$ and $\phi = 180°$ Amplitude Spectra Showing Effect of r_0 Error.

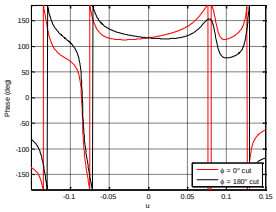

Figure 18. Comparison of $\phi = 0°$ and $\phi = 180°$ Phase Spectra Showing Effect of r_0 Error.

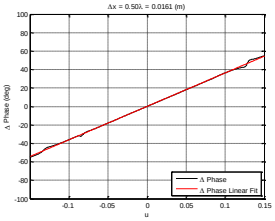

Figure 19. Difference Between Phase Spectra of $\phi = 0°$ and $\phi = 180°$ Cuts.

Here, it is assumed that $\phi = 0°$ and $\phi = 180°$ are parallel and anti-parallel respectively with the linear axis of the plane-polar near-field test system. Inspection of Figure 18 shows that, from the shifting properties of the Fourier transform, a linear phase taper has been introduced into the far-field pattern. The underlying linear phase function Δ, in radians, can be determined from the ratio of the respective spectra,

$$\Delta(u) = \text{imag}\left(\ln\left(\frac{F_0(u)}{F_{180}(-u)}\right)\right) \tag{5}$$

Here, imag is used to denote a function that returns the imaginary part of the argument, and ln is the natural logarithm. The slope of $\Delta(u)$ can be obtained numerically by performing a least squares fit to a linear phase function, $y = mx + C$ about the spectral region of greatest intensity. Once the gradient, m, of $\Delta(u)$ is known the linear displacement term can be obtained using,

$$r_0 = \Delta x = m/(2k_0) \tag{6}$$

Here, the additional factor of a half is included in the above equation as the displacement is obtained from the difference between the $\phi = 0°$ and $\phi = 180°$ cuts. As each individual cut contains the r_0 error, the phase difference will contain twice the expected error and this factor compensates for that. The displacement evaluation procedure set out above was verified for a number of measurement cases with the results being presented in Figure 19. Here, it was found that the algorithm correctly recovered the r_0 offset (a half wavelength for the case shown). However, it was also found that much smaller offsets could be reliably recovered with offsets a small as a twentieth of a wavelength (~1.6 mm at 9.375 GHz) being resolved. This data therefore confirms that calculation of a phase reference position based on two cuts ($\phi = 0°$ and $\phi = 180°$) taken from a single near-field acquisitions can provide a measure of the near-field r_0 error (error in the index offset) without the need to make auxiliary mechanical measurements. This type of calibration can be performed at a single frequency, and the information recovered can then be used for all subsequent measurements at all frequencies to correct for the alignment error. Whilst this method is not able to distinguish between probe translation and AUT translation, by repeating the measurement and instead rotating the probe by 180° a similar procedure can be used to determine and subsequently remove probe translation effects [10].

VII. Summary And Conclusions

A detailed mechanical alignment procedure has been presented using low cost alignment tools. A CEM simulation tool was developed to analyse the effects of r_0 radial position error on transformed far-field data. The simulation results show that for the 360° ϕ acquisition mode, the peak of the pattern has noticeably reduced as the r_0 error increased. It was evident that the peak level was far less sensitive to r_0 error for the 180° ϕ mode. Finally, a novel algorithm was developed that correctly recovered the r_0 offset using measured near-field data.

References

[1] D.M. Kerns, "Plane-Wave Scattering-Matrix Theory of Antennas And Antenna-Antenna Interactions", Nat. Bur. Stand. (U.S.) Monograph 162, June 1981.

[2] S.F. Gregson, J. McCormick, C.G. Parini, "Principles of Planar Near-Field Antenna Measurements", The Institution of Engineering and Technology, UK, 2007.

[3] V. Galindo-Israel, Y. Rahmat-Samii, R. Mittra, "A Plane-Polar Approach For Far-Field Reconstruction From Near-Field Measurements", Int. IEEE / AP-S Symp., Seattle, June, (1979).

[4] Y. Rahmat-Samii, L.I. Williams, R.G. Yaccarino, "The UCLA Bi-Polar-Near-Field Antenna-Measurement and Diagnostics Range", IEEE Antennas and Propagation Magazine, Vol. 37, No. 6, December, pp. 16-35, (1995).

[5] S.F. Gregson, A.C. Newell, G.E. Hindman, P. Pelland, "Range Multipath Reduction in Plane-Polar Near-Field Antenna Measurements", AMTA Symposium, Seattle, Washington, October 2012.

[6] A.C. Newell, "Error Analysis Techniques for Planar Near-field Measurements", IEEE Transactions on Antennas and Propagation, vol. AP-36, pp. 754-768, June 1988.

[7] A.C. Newell, G.E. Hindman, S.F. Gregson, "Antenna Pattern Comparisons used in NIST 18-Term Error Assessments on Numerous Near-field Ranges", 7th European Conference on Antennas and Propagation, 8-12 April 2013, Gothenburg, Sweden.

[8] A.C. Newell, G.E. Hindman, "The Alignment Of A Spherical Near-Field Rotator Using Electrical Measurements", AMTA Symposium, 1997.

[9] J. Demas, "Low Cost and High Accuracy Alignment Methods for Cylindrical and Spherical Near-field Measurement Systems", AMTA Symposium, 2005.

[10] D.J.v. Rensburg, "Compensation for Probe Translation Effects in Dual Polarized Planar Near-Field Antenna Measurements", AMTA Symposium, 2008.